The influence of in-plane constraints on fatigue crack growth rate

Jaroslaw Galkiewicz[1*] , Urszula Janus-Galkiewicz[1], Sebastian Lipiec[1]

[1] Faculty of Mechatronics and Mechanical Engineering, Kielce University of Technology, Aleja Tysiaclecia Panstwa Polskiego 7, 25-314 Kielce, Poland
* Corresponding author's e-mail: jgalka@tu.kielce.pl

ABSTRACT

The geometry of the structural members can influence the growth rate of fatigue cracks. Influence can be taken into account by incorporating dimensions into the formulas. However, such an approach is ineffective as the dependence of the crack growth rate is hard to predict and the formulas depend on the shape of the element. For each shape, a new formula is required. However, it is possible to use another approach that can be called a local approach in which the stress field parameters can be used in the neighborhood of the tip of the crack. It can be considered as an extension of Paris' approach to the growth of fatigue cracks. In the paper, the T-stress (the second term of Williams' solution) depending on the geometry of the element is used to quantify the effect of geometry on the growth rate of the fatigue crack. A series of fatigue in three-point bending specimens with different initial crack lengths. As a result, the dependence of the crack growth rate on the T-stress value was obtained.

Keywords: fatigue analysis, fatigue crack, Paris' law, in-plane constraints, brittle fracture, Williams' solution.

INTRODUCTION

In 1957 M.L. Williams [1] developed formulas for the stress distribution in front of the crack. The solution takes the form of a series of terms. Physical analysis allows one to limit the number of elements in a series, but still, there is a series of terms. In the vicinity of the crack tip, the components of the stress field can be described as follows.

$$\sigma_{xx} = \frac{K_I}{\sqrt{\pi r}} \cos\frac{\theta}{2}\left(1 - \sin\frac{\theta}{2}\sin\frac{3\theta}{2}\right) + T$$

$$\sigma_{yy} = \frac{K_I}{\sqrt{\pi r}} \cos\frac{\theta}{2}\left(1 + \sin\frac{\theta}{2}\sin\frac{3\theta}{2}\right)$$

$$\sigma_{zz} = \frac{K_I}{\sqrt{\pi r}} 2v\cos\frac{\theta}{2} + vT \qquad (1)$$

$$\sigma_{xy} = \frac{K_I}{\sqrt{\pi r}} \sin\frac{\theta}{2}\cos\frac{\theta}{2}\cos\frac{3\theta}{2}$$

$$\sigma_{xz} = \sigma_{yz} = 0$$

where: σ_{xx}, σ_{yy}, σ_{zz}, σ_{xy} – stress tensor components, K_I is the stress intensity factor (SIF), v is Poisson's ratio, E is Young's modulus, θ (angle created with x-axis) and r (distance from origin) are the coordinates of the polar system with origin located at the tip of the crack, and T is the second term of the series expansion that represents the stress acting parallel to the cracked plane.

Usually, only the first dominant term was used to describe the stress field in the vicinity of the crack tip [2]. In his analysis, Williams assumed that the body is infinite. In reality, a body has finite size and shape that influence the fracture toughness. This was taken into account in the standard [3] by strict requirements for the shape and dimensions of a specimen for the test to be valid. In 1973 Larsson and Carlsson [4] showed that the size and shape of the plastic zone ahead of the crack tip depends on the in-plane geometry of the specimen. The influence of the specimen geometry can be considered by the value of the T-stress, which is the second term of Williams' expansion (1).

In the case of elastic-plastic materials, the stress field may be described by the Hutchinson, Rice, and Rosengren equations [5, 6]. They describe the so-called HRR (Hutchinson, Rice, and Rosengren) field. In this case, there is also the quantity that is equivalent to the T-stress. The complete solution for the HRR field was given by Yang et al. [7], but the Shih and O'Dowd approach turned out to be more popular, mainly due to its simplicity [8–11]. In this case, the equivalent of the T-stress is the Q-stress, which is the sum of all higher-order elements of the asymptotic expansion. In [9] is given the simple relationship between fracture toughness and Q-stress value.

The influence of in-plane constraints on the fatigue process in the crack initiation phase and in the ultra-low-cycle fatigue range was shown in [12] and [13]. These articles showed that the T-stress (or Q-stress) level affects not only the fatigue crack growth rate and the number of cycles to crack initiation but also the crack initiation site.

The fatigue crack growth rate is strictly related to the stress intensity factor. The first person who saw it was P.C. Paris. From that time there were many crack growth equations proposed but the most popular and comprehensive is still Paris' law [14], which can be written as:

$$\frac{da}{dN} = C\left(\Delta K_{eff}\right)^m \tag{2}$$

where: da/dN is the crack growth in millimeters per cycle, C and m (parameters of the Paris' law) are the material constants,

$$\Delta K_{eff} = \left(\frac{1}{1-R} - \frac{\Delta K_{op}}{\Delta K}\right)\Delta K \tag{3}$$

where: ΔK is a range of the stress intensity factor (SIF) changes, ΔK_{op} is the SIF value when crack starts to open, R is a stress ratio which in this case is the ratio of the minimum to maximum stress intensity factors.

As a result of Equation 3, the rate of increase in fatigue crack depends primarily on the load, which affects the range of changes in the stress intensity factor, but also on the stress ratio, i.e. the average load [15–17]. The last quantity is the threshold value of the stress intensity factor at which the crack opens. Unfortunately, the fatigue cracking process is too complicated to be described by formula (2) alone. Therefore, research in the current stage of scientific development tries to take into account other factors. One of the elements that are difficult to describe mathematically is the effect of the environment. In article [18], the effect of humidity and temperature was studied simultaneously. This effect was included by describing the changes in the parameters C and m in the Paris' law.

In the article [19] W. Macek studied the influence of the stress ratio on the roughness of the crack surface. It turns out that the surface roughness is significantly affected by the stress ratio, and the roughness parameters change their values as the crack increases. It suggests that surface roughness can be used to identify the stage of crack growth, and, on the other hand, roughness itself influences the crack growth rate.

In [20] the authors investigated the low cycle fatigue range. They proved that surface parameters can be applied to assess the fatigue life of cracks. They used the total strain energy density and some topography parameters of the fractured surface to successfully assess fatigue life.

Much more difficult to control is the effect of an aggressive environment [21]. In such a case, the simplest tool to show the effect of the selected factor is the Paris' equation plot.

It is equally difficult to describe the effect of the microstructure of the material on the crack growth rate. For example, in [22] the effect of microstructure on the crack initiation site and the path of the growth of fatigue cracks in welded joints was analyzed. In [23] many aspects of the growth of fatigue cracks in railway rails were studied, and one of the elements taken into account was the grain size. It was found that a finer microstructure requires a greater number of cycles to failure, and thus reduces the crack growth rate. In [24] the effect of the inhomogeneity of the structure (clusters of small grains near large grains) was studied at the fatigue crack initiation site, as well as on how the structure affects crack growth in its initial phase.

The influence of individual parameters can be enhanced by their mutual influence [25], which is why artificial intelligence is increasingly used to assess the influence of selected parameters on the fatigue process [26, 27].

The influence of parameters that are much easier to describe mathematically is the influence of material properties on fatigue behavior [28]. Another parameter not directly taken in the formulas even though its influence is as obvious as those mentioned before is geometry. The material or its properties can be changed. However, the

requirements of an engineering problem force the geometry of the element. In general, the shapes of the machine members differ from those of laboratory specimens. Arbitrary geometry makes it hard to predict fatigue behavior. Geometry influences the state of stress and strain. As a result, fatigue behavior is not intuitive. The other problem is that there is no parameter that can define the influence of the shape and dimensions of structural members. Universal parameters applied in the mathematical formulas would allow for the direct transfer of results from the laboratory to engineering practice in an easy way.

The growth of the crack may differ significantly from the model described by the Paris' law, calculated in the laboratory using standard specimens. The main reason is geometry, because the material used in the tests is usually the same as the one from which the structural element is made.

The influence of geometry is divided into two groups due to the constraints that geometry imposes on the development of plastic zones. The influence of thickness on the growth rate of fatigue cracks was tested in [29] and [30]. Thickness creates the so-called out-of-plane constraints. The shape and dimensions of the element, in turn, constitute the second group of constraints, i.e., in-plane constraints.

The influence of the shape and dimensions of the elements on the behavior of fracture and fatigue was already noticed. In flawless elements, the theoretical stress concentration factor, fatigue stress concentration factor, and notch sensitivity factor can be applied to evaluate fatigue life. However, in this case, different formulas are used for each geometry. The formulas can be found in books, for example [31]. That is why in the FIT-NET procedures [32] the normalized stress gradient is used. Thanks to that, the same formulas are used for any shape. In the case of fracture mechanics, the problem was solved differently. Standards for the evaluation of fracture toughness require specimens dominated by plane strain conditions, which results in highly constrained geometries allowed for the test. The fracture toughness of arbitrary elements is evaluated by taking into account T-stress or Q-stress.

There is an acknowledged influence of geometry-induced constraints in fracture cases (monotonic loads) and in fatigue loads, but for flawless geometries. Logically, the same should be found in the case of fatigue crack growth problems. In view of the findings of Larsson and Carlsson [4]

combined with the results of O'Dowd [9] in the field of monotonic loading, it seems quite obvious to try to use a two-term approach to describe the growth of fatigue cracks. An additional advantage of such an approach would be a uniform approach to the influence of geometry. Regardless of the shape of the element, the influence of geometry would be described by the same equations. It would be possible because instead of a global approach that takes into account details of geometry, a local approach that takes into account the influence of any geometry on the crack tip stress field defined by SIF and T-stress is proposed. The T-stress is the parameter that describes the influence of geometry in this case.

It was noticed that T-stress could help describe differences in fatigue behavior due to geometry. In [33], the rate of fatigue crack growth is explained with the strain energy density, which can be treated as a form of energy-based approach to describe different aspects of fatigue. What is important about the strain energy density is that its value can be expressed as a function of T-stress, so in fact, fatigue crack growth is indirectly dependent on T-stress. Tong in [34] investigated fatigue crack growth rates for different geometries. Differences in crack growth rates were obvious. The author found that in the case of elastic-plastic materials, lower values of T-stress (or Q-stress as its equivalent in the J-Q approach) lead to lower crack growth rates. In the three-dimensional case, the highest T-stress values along the crack front are obtained in the center of the specimen, which leads to the effect of tunneling as the crack growth increases.

This scientific paper presents preliminary studies of fatigue crack growth rates for different levels of in-plane constraints. In the experiments, three-point bending specimens with different crack lengths will be used. This allows us to load specimens to the same level of the SIF but for different levels of T-stress. The T-stress depends in this case only on the crack length and is easily evaluated using the finite element method. In such an arrangement, the only parameter that influences crack growth is the level of geometrical constraints defined by theT-stress. In the first stage, when the crack increases from 0 to 1 mm, the differences obtained fit the T-stress values very well. For the second stage, when the crack grows from 1 to 2 mm, the stress intensity factor exceeds the critical values, and the specimen should break in such a case. However, if the level of constraint is sufficiently high, it does not

happen, which is surprising because it is not consistent with the Paris' law but can be explained using any criteria. In our case, we used the Tresca criterion.

EXPERIMENTAL PROCEDURE

The tests were carried out on specimens made of C45 steel (1.0503 (PN-EN 10027-2)/ 1045 (AISI)). Tensile tests and fracture toughness tests were performed on the MTS 250 servohydraulic system, while fatigue tests were performed on the MTS 100 servohydraulic system. The values of material constants achieved in the tensile tests are presented in Table 1 and Figure 1a. The fatigue load amplitude was made to depend on the critical value of the stress intensity factor. To determine it, three three-point bending specimens are prepared with a thickness of $t = 10$ mm and other dimensions proportional to this thickness according to the standard [3]. As a result of the experiments, an average value of $K_{IC} = 53,5$ MPa√m was obtained (K_{IC}– critical value of the stress intensity factor).

The next step was to make a set of three-point bending specimens with a thickness of $t = 10$ mm and other dimensions according to the standard [3] except for the length of the crack. Three different crack lengths are introduced into the specimens to obtain the relative crack length $a/W = 0.25, 0.5, 0.75$, where a is the crack length and W is the width of the specimen. The samples were

subjected to fatigue loading with repeated cycles of two maximum values: $0.77K_{IC}$ and $0.5K_{IC}$, while the minimum value was always the same and equal to 0.1 kN. A zero force value was not used due to the possibility of loss of contact between the actuator and the specimen. The force values corresponding to the maximum SIF levels assumed were determined as follows [35]:

$$P = \frac{K_I 2tW^2}{3S\sqrt{\pi a}F_I(\alpha)} \quad (4)$$

where: $\alpha = a/W$, $F(\alpha) = \frac{1.99 - \alpha(1-\alpha)(2.15 - 3.93\alpha + 2.7\alpha^2)}{(1+2\alpha)(1-\alpha)^{1.5}}$

and the remaining parameters W– specimen width, P – load, S – specimen span, a – crack length, and t – thickness of the specimen are defined in Figure 2,

The number of cycles in which the crack growth reached 1 mm and 2 mm was recorded. Crack growth measurements were made optically

Table 1. Material parameters

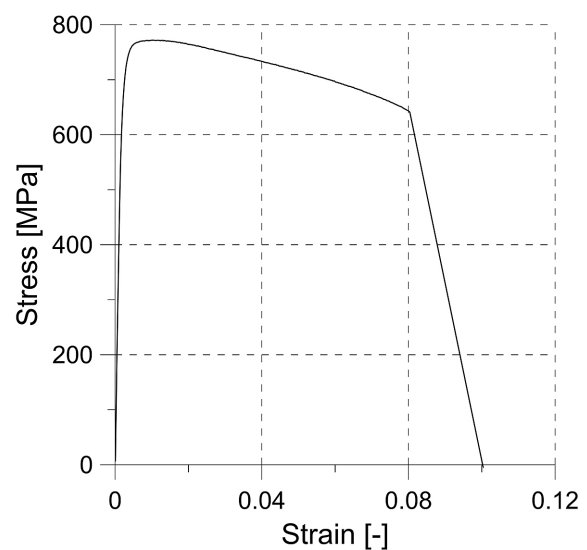| Feature	Value
Young's modulus [GPa]	182.9
Yield strength [MPa]	711.45
Tensile strength [MPa]	771.61
Elongation [%]	16
Reduction in area [%]	64.54

Figure 1. Examples of the results of the tensile test (ISO 6892-1) (a) and of the determination of the critical stress intensity factor (ASTM E399) (b).
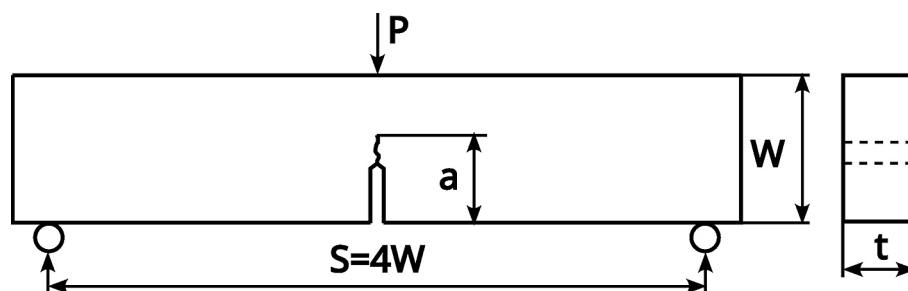

Figure 2. Geometry of the tested specimens

on the surface of the specimens. First, on the face of each specimen, two lines were scratched to mark the distances (1 mm and 2 mm) from the initial crack tip (Fig. 3). Then using Olympus SZX2 a crack growth was observed until the crack tip reached the line. The maximum forces used to load the samples are shown in Table 2.

Experimental results

During the tests, the number of cycles was recorded after reaching an increase of 1 mm and 2 mm. The measurement results were an average of three samples. Tables 3 and 4 show the average results of the measurements of the number of cycles required to achieve the assumed increase. As seen, the number of cycles required to achieve a 1 or 2 mm increase in the crack is lower for greater loads, which is obvious, but the number of cycles is greater for longer cracks. In the case of the longest cracks, that is, $a/W = 0.75$, it was not possible to determine the average. In the case of the lower load level, no increase was observed or it was very small, therefore the tests were stopped after exceeding 1,000,000 cycles, but at a higher load level, one of the specimens broke suddenly before reaching an increase of 2 mm.

NUMERICAL PROCEDURE

To explain the results obtained, the T-stress values are used as it is the only parameter in the experiment that changes. To determine the T-stress values, numerical calculations performed in the ABAQUS/CAE 2017 program were used. The specimens were modeled in plane strain using 4-node bilinear elements (CPE4R). Taking advantage of the problem symmetry, only half of the specimen is modeled. In each specimen, the zone in the vicinity of the crack is modeled as a rectangle composed of two squares filled with elements of size 0.003×0.003 mm (Fig. 4). The size of the elements near the crack tip guarantee stable and accurate results. The model is composed of over 230 thousand elements. The exact number depends on the length of the crack. For $a/W = 0.25$ and $a/W = 0.75$, it was 236,000 elements; for $a/W = 0.5$, it was 236,000 elements. The loading roller and the support roller were modeled as rigid bodies. The displacement was applied to the appropriate roller. Its value is sufficient to obtain the required K-values. The T-stress values
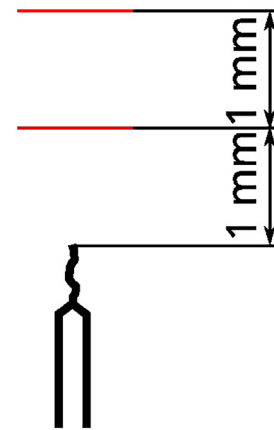

Figure 3. The scheme to measure the growth of cracks

were determined automatically by the ABAQUS program.

To validate results, calculations were repeated with elements of three times greater size, that is, 0.009×0.009 mm. The results differ by 0.67% and 0.16% for T-stress and K_I-value respectively. The values obtained prove that the elements used are sufficiently small.

Numerical results

The T-stress values at the beginning of the load for each load case determined by numerical calculations are presented in Table 5. As can be seen, the T-stress in the crack plane can be positive or negative. For the crack plane, θ is equal to

Table 2. Applied loads [N]

Max. SIF level	a/W=0.25	a/W=0.5	a/W=0.75
0.5 K_{IC}	3985	2004	692
0.77 K_{IC}	6161	3098	1070

Table 3. Number of cycles to achieve 1 mm crack growth

Max. SIF level	a/W=0.25	a/W=0.5	a/W=0.75
0.5 K_{IC}	63793	113274.5	>10⁶
0.77 K_{IC}	25855	29477.5	90706

Table 4. Number of cycles to achieve 2 mm crack growth

Max. SIF level	a/W=0.25	a/W=0.5	a/W=0.75
0.5 K_{IC}	117969	185015	>10⁶
0.77 K_{IC}	43713	49085	not conclusive

Table 5. T-stress values [MPa]

Max. SIF level	a/W=0.25	a/W=0.5	a/W=0.75
0.5 K_{IC}	-38.65	19.09	67.55
0.77 K_{IC}	-59.75	29.49	104.43

zero. In this case, the equation (1) for σ_{xx} (stress tensor component) reduces only to *T*. This means that the T-stress is a value of the stress σ_{xx} acting in the crack plane, which can be compressive or tensile. Lower values are obtained for shorter cracks and higher loads. As a result, the highest T-stress value is obtained for *a/W* = 0.75, and the load level 0.77K_{IC}, while the lowest value corresponds to the shortest crack, that is, *a/W* = 0.25

and the load level 0.5K_{IC}. The T-stress values perfectly fit the number of cycles to reach the assumed increase of a crack presented in Tables 3 and 4. The higher the value of T-stress, the lower the crack growth rate.

DISCUSSION

In all cases, the initial load had the same parameters. Both the maximum load value and the stress ratio are identical, nevertheless, the number of cycles to achieve the intended increments is clearly different (Fig. 5). The only quantity that has different values at the beginning of the
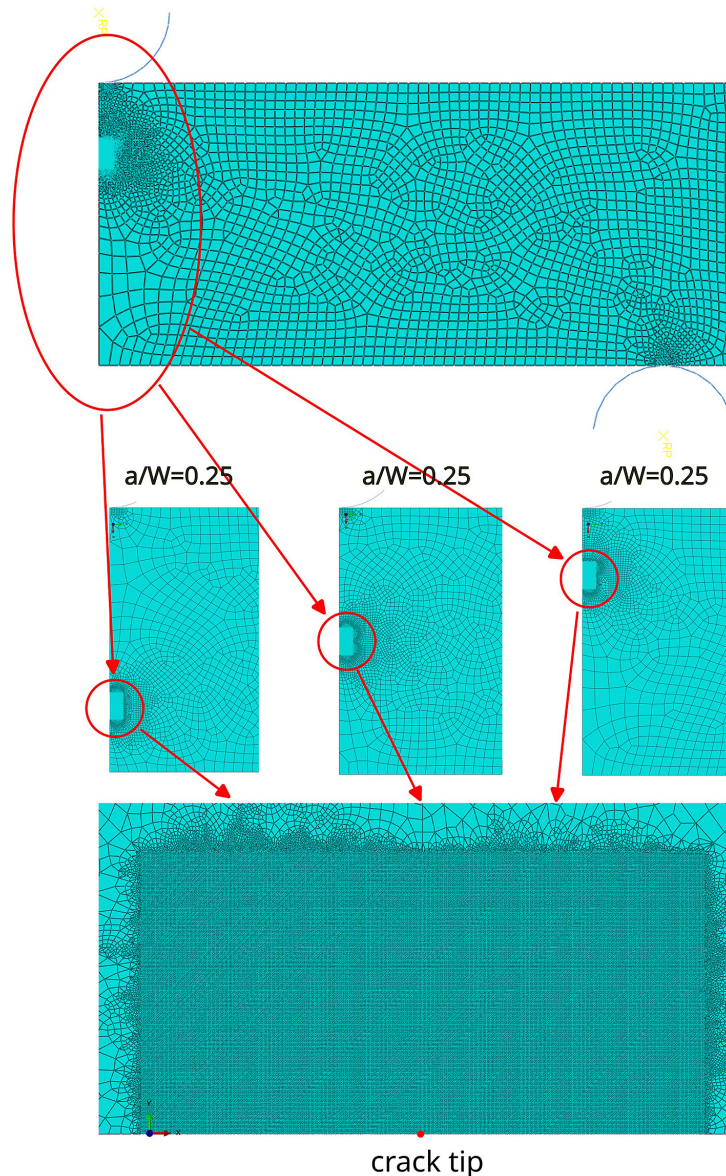

Figure 4. Details of the numerical model: general view of the specimen (top row), area of the plane of symmetry (middle row), and crack tip zone (bottom row)
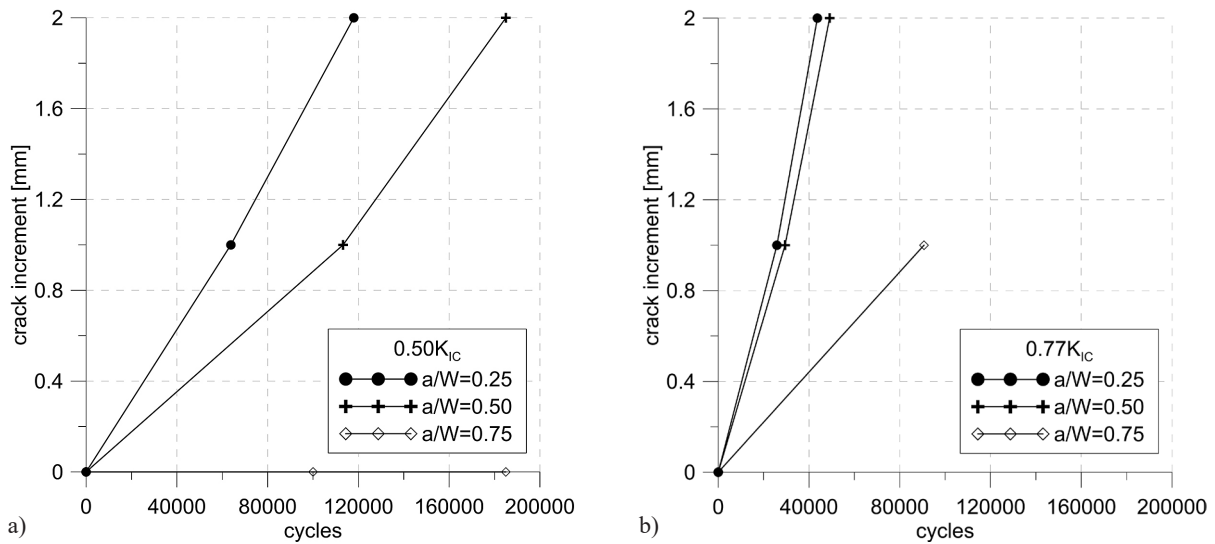
Figure 5. Graphical presentation of the results of Tables 3 and 4

experiments is the T-stress. The crack growth rate in Figure 5 is expressed by the slopes of the lines. In the range of increase of 0–1 mm, the crack growth rate is lower than for the range of 1–2 mm for both load cases.

The change in the rate of growth of the crack is caused by the increasing value of the stress intensity factor. According to formula (4) the stress intensity factor depends on the length of the crack and the force applied to the specimen. As the maximum applied force is constant, only the growth of the crack causes an increase in the SIF value. The maximum SIF values for assumed crack increments are shown in Tables 6 and 7.

As can be seen in Tables 6 and 7, an increase in the SIF value is greater for longer crack growths. In the case of a load level equal to 0.77 K_{IC} for a crack growth of 2 mm, the SIF is equal to or greater than the critical value. According to the Paris' law, crack growth should reach a catastrophic

rate. The crack growth rate, however, behaves oppositely, which is unexpected. The specimens did not fail rapidly except for one sample with *a/W* = 0.75. However, in this case, the SIF exceeded the critical value by 67%. This geometry should already have failed for an increase of 1 mm, corresponding to an increase in SIF to 58 MPa√m (Table 6). This could be attributed to the influence of the constraint on crack tip closure. As shown in [13], positive T-stress reduces plastic deformation at the tip of the crack and reduces the value of the opening stress intensity factor, leading to an increased effective range of the SIF. However, since the applied load is low, the effect of crack closure in this case is considered negligible, similarly to [34].

Comparing the obtained increases with the T-stress values, a close correlation can be seen. Specimens with a higher T-stress value were characterized by lower fatigue crack growth rates or their arrest, while low values promoted acceleration of crack growth (Tables 8 and 9).

It is noticed that the results can be explained by adopting a failure theory. The Tresca criterion was selected. In this theory, failure occurs when the maximum shear stress value reaches the

Table 6. SIF values for the length of the crack increased by 1 mm [MPa√m]

Max. SIF level	a/W=0.25	a/W=0.5	a/W=0.75
0.5 K_{IC}	30.4	31.6	37.5
0.77 K_{IC}	46.0	48.8	58.0

Table 7. SIF values for the length of the crack increased by 2 mm [MPa√m]

Max. SIF level	a/W=0.25	a/W=0.5	a/W=0.75
0.5 K_{IC}	34.6	37.9	57.9
0.77 K_{IC}	53.5	58.6	89.5

Table 8. Crack growth rates in the range 0–1 mm [mm/cycle]

Max. SIF level	a/W=0.25	a/W=0.5	a/W=0.75
0.5 KIC	1.57E-05	8.83E-06	arrested
0.77 KIC	3.87E-05	3.39E-05	1.10E-05

critical value. The value of maximum shear stress depends on the principal stresses:

$$\tau_{max} = \max\left(abs(\sigma_1 - \sigma_2), abs(\sigma_1 - \sigma_3), abs(\sigma_2 - \sigma_3)\right) \quad (5)$$

According to Equations 1, all shear stresses in the fracture plane equal zero, so normal stresses become the principal stresses. This behavior can

Table 9. Crack growth rates in the range of 1–2 mm [mm/cycle]

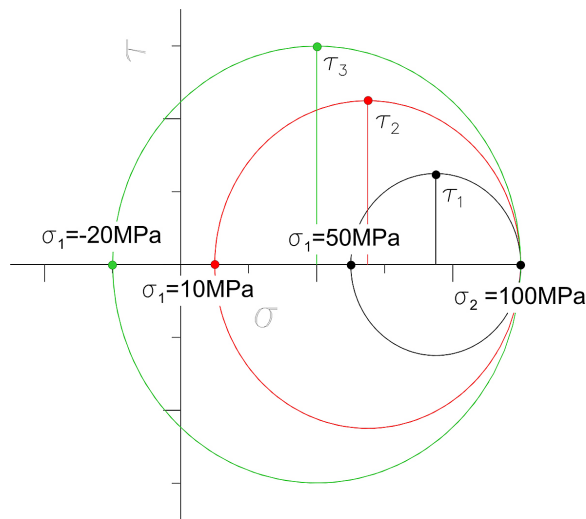| Max. SIF level	a/W=0.25	a/W=0.5	a/W=0.75
0.5 K_{IC}	1.85-05	1.39-05	arrested
0.77 K_{IC}	5.6E-05	5.10E-05	not conclusive

Figure 6. Mohr circles for selected values of T-stress: T = -20 MPa (green circle), T = 10 MPa (red circle), and T = 50 MPa (black circle)
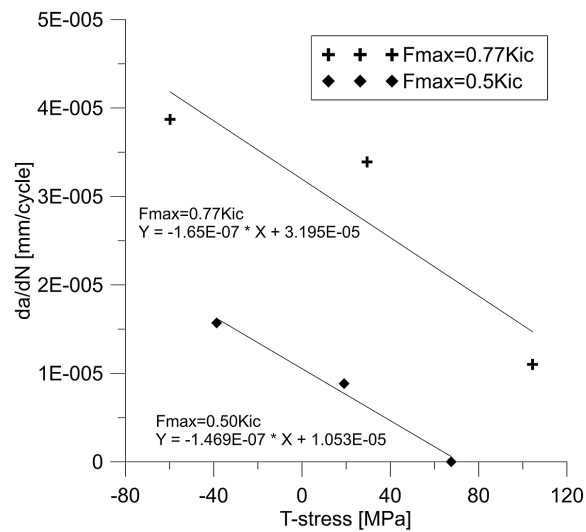

Figure 7. Relation between T-stress and crack growth rate

be explained by the influence of the level of in-plane constraints on the value of the principal stresses. In the case of plane strain, the stresses in the thickness direction are equal $\sigma_3 = (\sigma_1 + \sigma_2)\nu$ where ν is Poisson's ratio, σ_3 is the principal stress in thickness direction, and σ_1, σ_2 (principal stresses) are the principal stresses in the other directions (i.e., in the specimen plane) and therefore the maximum shear stress depends on the stresses σ_1 and σ_2 (6).

$$\tau_{max} = \sigma_2 - \sigma_1 \quad (6)$$

In the case considered, on the crack growth path, the stress level σ_2 depends on the SIF value while σ_1 is equal to the T-stress. As can be seen in Fig. 6, the value of maximum shear stress depends on the T-stress. The lower the T-stress value, the higher the maximum shear stress.

CONCLUSIONS

The tests were carried out in which specimens with different levels of T-stress were loaded with repeating cycles of the same amplitude of SIF. Increased crack length results in an increasing value of the stress intensity factor. In some cases, the SIF significantly exceeded the critical value, but the specimen did not break. Different crack growth rates were obtained for each geometry for two levels of loading. These rates are correlated with the level of in-plane constraints described by the T-stress values. The lower the T-stress, the greater the growth rate of fatigue cracks.

The results indicate the need to introduce a quantity characterizing the in-plane constraints into the crack growth function, as it has a strong influence on the behavior of the fatigue crack. In the case of fatigue crack growth Paris' law uses ΔK (2) but as shown it can be an imprecise approach. The solution may be the participation of the T-stress in the Paris' formula:

$$\frac{da}{dN} = f(\Delta K, T) \quad (7)$$

Determining the exact structure of (7) requires significantly more results. It is planned to test the growth of fatigue cracks for specimens subjected to tensile and bending loads.

The introduction of T-stress is very tempting, as this parameter gets different values for specimens of different shapes and sizes. Therefore, it will allow one to use the same formulas for crack growth for any geometry. The positive results of

future experiments will allow an easy transfer of the Paris' curve to any geometry using only a simple FEM calculation.

REFERENCES

1. Williams, M. L. On the stress distribution at the base of a stationary crack, Journal of Applied Mechanics, 1957; 24, 109–114.

2. Anderson, T. L. Fracture Mechanics: Fundamentals and Applications, Boca Raton: CRC Press, 1994.

3. ASTM E. Standard Test Method for Plane- Strain. Fracture Toughness of Metallic Measurment, West Conshohocken, PA: ASTM International, 1997, 399–90.

4. Larsson S. G. and Carlsson A. J. Influence of non-singular stress terms and specimen geometry on small-scale yielding at crack tips in elastic-plastic materials, Journal of Mechanics and Physics of Solid, 1973; 21, 263–277.

5. Hutchinson, J. W. Singular behaviour at the end of a tensile crack in a hardening material, Journal of the Mechanics and Physics of Solids, 1968; 16, 13–31.

6. Rice, J. R. and Rosengren, G. F. Plane strain deformation near crack tip in a power-law hardening material, Journal of the Mechanics and Physics of Solids, 1968; 16, 1–12.

7. Yang, S., Chao Y. and Sutton M. Higher order asymptotic crack tip fields in a power-law hardening material, Engineering Fracture Mechanics, 1993; 19(1), 1–20.

8. O'Dowd, N. and Shih, C. Family of crack-tip fields characterized by a triaxiality parameter – I. structure of fields, Journal of the Mechanics and Physics of Solids, 1991; 39(8), 989–1015.

9. O'Dowd, N. and Shih, C. Family of crack-tip fields characterized by a triaxiality parameter – II. fracture applications, Journal of the Mechanics and Physics of Solids, 1992; 40(5), 939–963.

10. O'Dowd, P.N. Application of two parameter approaches in elastic–plastic fracture mechanics, Engineering Fracture Mechanics, 1995; 52(3), 445–465.

11. O'Dowd, N., Shih C. and Dodds, R. J. The Role of Geometry and Crack Growth on Constraint and Implications for Ductile/Brittle Fracture, in Constraint Effects in Fracture Theory and Applications: Second Volume, Philadelphia, 1995.

12. Janus-Galkiewicz, U. and Galkiewicz, J. Analysis of the failure process of elements subjected to monotonic and cyclic loading using the Wierzbicki–Bai Model, Materials, 2021; 14(6265).

13. Galkiewicz, J. and Janus-Galkiewicz, U. The numerical analysis of the in-plane constraint influence on the behavior of the crack subjected to cyclic loading, Materials, 2021; 14(1764), 1–14.

14. Paris', P., Gomez, M. and Anderson, W. A rational analytic theory of fatigue, The Trend in Engineering, 1961; 13, 9–14.

15. Simon, I., Banks-Sills, L. and Fourman, V. Mode I delamination propagation and R-ratio effects in woven composite, International Journal of Fatigue, 2017; 96, 237–251.

16. Zhu, J., Xu, L. and Guo, W. The influence of bending loading on surface fatigue crack growth life, International Journal of Fatigue, 2023; 167(107285).

17. Bilir, O. G. and Harun, M. Effect of stress ratio on the rate of growth of fatigue cracks in 1100 Al-alloy, Engineering Fracture Mechanics, 1990; 37(6), 1203–1206.

18. Alqahtani, I., Starr, A., Khan, M. Investigation of the combined influence of temperature and humidity on fatigue crack growth rate in Al6082 alloy in a coastal environment. Materials 2023; 16, 6833. https://doi.org/10.3390/ma16216833

19. Macek, W. Fracture surface formation of notched 2017A-T4 aluminium alloy under bending fatigue, International Journal of Fracture, 2022; 234, 141–157.

20. Macek, W., Branco, R., da Silva, J. A. de Jesus, S.-P., Zhu, R. Masoudi Nejad and Gryguc, A. Strain energy density and entire fracture surface parameters relationship for LCF life prediction of additively manufactured 18Ni300 steel, International Journal of Damage Mechanics, 2024; 33(7), 725–747.

21. Free, B., Marino, G., Schindelholz, E., Dorman S. G. and (Warner) Locke, J. S. Measurement of atmospheric corrosion fatigue crack growth rates on, International Journal of Fatigue, 2023; 167, Part A, 107368, https://doi.org/10.1016/j.ijfatigue.2022.107368

22. Meng, X., Yang, S., Huang, Y., Fang, Y., Gu, J., Xiong, Q. and Duan, C. Microstructure characterization and mechanism of fatigue crack propagation of 6082 aluminum alloy joints, Materials Chemistry and Physics, 2021; 257, 123734.

23. Yang, B., Wang, S., Li, J., Ding, X., Xiao, Q. and Xiao, S. Study on fatigue crack growth in rail steel at numerical and, Materials, 2023; 16(2981).

24. Li, X., Liu, C., Wang, X., Dai, Y., Zhan, M., Liu, Y., Yang, K., He, C. and Wang, Q. Effect of microstructure on small fatigue crack initiation and early propagation behavior in super austenitic stainless steel 654SMO, International Journal of Fatigue, 2024; 179(108022).

25. Alberto Carpinteri, M. P. Are the Paris' law parameters dependent on each other?, Frattura ed Integrità Strutturale, 2007; 2, 10–16.

26. Omar, I., Khan, M. and Starr, A. Comparative analysis of machine learning models for predicting crack propagation under coupled load and temperature, Applied Sciences, 2023; 13(7212).

27. Susmel, L. Estimating notch fatigue limits via a machine learning-based approach structured according to the classic Kf formulas, International Journal of Fatigue, 2024; 179(108029).

28. Remmal, A. and Leblond, J.-B. Ductile rupture under cyclic loadings at high triaxiality: The influence of strain hardening and elasticity, Mechanics of Materials, 2024; 192(104982).

29. Calvin, G., Escalero, M., Zabala, H. and Muñiz-Calven, M. Distribution of the through-thickness effective stress intensity factor range and its influence on fatigue crack growth rate curves, Theoretical and Applied Fracture Mechanics, 2022; 119(103374).

30. Burns, J. T., Boselli, J. Effect of plate thickness on the environmental fatigue crack growth behavior of AA7085-T7451, International Journal of Fatigue, 2016; 83, 253–268.

31. Pilkey, W. D. and Pilkey, D. F. Peterson's Stress Concentration Factors, Third Edition, Hoboken, New Jersey: John Wiley & Sons, Inc., 2008.

32. Janosch, J., Huther, M., Kocak, M. and Taylor, N. European Fitness for Service Network (FITNET) "Fatigue Module Development". In: Proceedings of the 24th International Conference on Offshore Mechanics and Arctic Engineering, New York, 2005.

33. Ayatollahi, M. R., Rashidi Moghaddam, M. and Berto, F. T-stress effects on fatigue crack growth – Theory and experiment, Engineering Fracture Mechanics, 2018; 187, 103–114.

34. Tong, J. T-stress and its implications for crack growth, Engineering Fracture Mechanics, 2002; 69, 1325–1337.

35. Murakami, Y. Stress Intensity Factors Handbook, Volume 1, Oxford: Pergamon Press, 1987.